Atmos. Chem. Phys., 22, 9513–9524, 2022
https://doi.org/10.5194/acp-22-9513-2022

Atmospheric Chemistry and Physics
Open Access
EGU

Measurement report: On the contribution of long-distance transport to the secondary aerosol formation and aging

Haobin Zhong[1,2], Ru-Jin Huang[1,2,3,7], Chunshui Lin[1], Wei Xu[1], Jing Duan[1], Yifang Gu[1,2], Wei Huang[1], Haiyan Ni[1], Chongshu Zhu[1], Yan You[4], Yunfei Wu[5], Renjian Zhang[5], Jurgita Ovadnevaite[6], Darius Ceburnis[6], and Colin D. O'Dowd[6]

[1]State Key Laboratory of Loess and Quaternary Geology, Center for Excellence in Quaternary Science and Global Change, Institute of Earth Environment, Chinese Academy of Sciences, Xi'an 710061, China
[2]University of Chinese Academy of Sciences, Beijing 100049, China
[3]Open Studio for Oceanic-Continental Climate and Environment Changes, Pilot National Laboratory for Marine Science and Technology (Qingdao), Qingdao 266061, China
[4]National Observation and Research Station of Coastal Ecological Environments in Macau, Macau Environmental Research Institute, Macau University of Science and Technology, Macau SAR 999078, China
[5]Key Laboratory of Middle Atmosphere and Global Environment Observation (LAGEO), Institute of Atmospheric Physics, Chinese Academy of Sciences, Beijing 100029, China
[6]School of Physics and Ryan Institute's Centre for Climate & Air Pollution Studies, National University of Ireland Galway, University Road, Galway H91CF50, Ireland
[7]Institute of Global Environmental Change, Xi'an Jiaotong University, Xi'an 710049, China

Correspondence: Ru-Jin Huang (rujin.huang@ieecas.cn)

Received: 11 April 2022 – Discussion started: 18 May 2022
Revised: 30 June 2022 – Accepted: 4 July 2022 – Published: 22 July 2022

Abstract. To investigate the physio-chemical properties of aerosol transported from major pollution regions in China, observations were conducted ∼200 m above the ground at the junction location of the North China Plain and Fenwei Basin, which are two regions of top priority for China's Blue Sky Campaign. We identified three pollution transport sectors including those from Beijing–Tianjin–Hebei (BTH), urban Guanzhong Basin (GZB) and northern China and one clean transport sector from the rural Guanzhong Basin region. Secondary inorganic aerosol (SIA) constituted a major fraction (39 %–46 %) in all pollution transport sectors, with a high sulfur oxidation ratio (0.44–0.58) and a high nitrogen oxidation ratio (0.24–0.29), suggesting efficient formation of secondary inorganic aerosol during regional transport. More oxidized oxygenated organic aerosol (MO-OOA) played a dominant role in the source of organic aerosol in all sectors including the clean one, accounting for 42 %–58 % of total organic aerosol. Elemental analysis (O and C) shows that aerosol particles at this receptor site were much more oxidized than in urban regions, pointing that long-range transport contributed markedly to the organic aerosol oxidation and aging. Case studies of pollution events with high sulfate, nitrate and more-oxidized oxygenated organic aerosol production rate indicate the strong formation efficiency of secondary aerosol during regional transport in the Beijing–Tianjin–Hebei transport sector.

Published by Copernicus Publications on behalf of the European Geosciences Union.

1 Introduction

Air pollution events with high levels of fine particles (particulate matter with a diameter $\leq 2.5\,\mu m$, $PM_{2.5}$) have frequently occurred in China over the past years, due to rapid industrialization and urbanization (Lelieveld et al., 2015; Feng et al., 2018; An et al., 2019). The high level of $PM_{2.5}$ affects air quality, human health and the climate and thus has received widespread concern around the world (Tie et al., 2016; Cohen et al., 2017). To better understand air pollution in China, many field studies have been carried out in the last decades (Tie and Cao, 2009; Lei et al., 2011; Cao et al., 2012; Huang et al., 2014; Liu et al., 2018). Most of these studies for particle properties are based on local observations, such as in Beijing (Sun et al., 2013; Li et al., 2019), Shanghai (Xu et al., 2012; Y. Huang et al., 2013; Wang et al., 2020), Xi'an (Huang et al., 2014; Duan et al., 2021; Lin et al., 2022), Guangzhou (Guo et al., 2020; Chen et al., 2021) and Hong Kong (Li et al., 2015; Sun et al., 2016). However, aerosol particles can affect areas hundreds of kilometers away through transport, depending on particle size and chemical compositions (Uno et al., 2009). During transport, aerosols undergo further transformation, altering chemical composition and oxidation level and consequently affecting their physico-chemical properties and climate impact (Moffet and Prather, 2009; Riemer and West, 2013; Calvo et al., 2013; Fierce et al., 2016).

Recent studies found that local formation cannot fully explain the increase in SIA during pollution events, and the regional transport was considered an important source for the increase in SIA (Yang et al., 2015; Tang et al., 2016). Some modeling studies reported that heterogeneous chemistry during transport was identified as the dominant factor during haze episodes in megacities (Li and Han, 2016; Li et al., 2017) and were further supported by the observations. Du et al. (2019) reported that the chemical transformation from SO_2 to sulfate was the major source of sulfate in Beijing. Li et al. (2021b) suggested that the pollution in winter in Beijing was largely affected by regional transport, and water vapor during transport of the air mass greatly increased the SIA proportion. Gunsch et al. (2018) claimed that the particles were heavily coated with secondary organic aerosol (SOA) formed during transport, with PM_1 being 89 % organics and a O / C ratio of 0.8 in the forested Great Lakes region in the United States during the wildfire period. Most of the existing studies were devoted to studying the contribution of regional transport to pollution events in urban areas, while studies on region-to-region transport were limited. Our previous study reported that different regions in China represented different chemical compositions and OA sources due to different types of emission characteristics (Zhong et al., 2020). Therefore, the transport aerosol particles from different regions may have completely different properties due to different precursors and transport conditions. The study of region-to-region transport can provide insight into the interactions and mixing properties of particles on a national scale.

Investigation of the chemical compositions and sources with the transport pathways in background areas is a common method to understand the influence of long-distance transport of aerosol on the atmospheric environment (Schichtel et al., 2006; Salvador et al., 2008; Das and Jayaraman, 2012; Tang et al., 2014; Pu et al., 2015). In this study, we performed a 1-month observation at a regional receptor site to investigate the characteristics of aerosol transported from major pollution regions by using a time-of-flight aerosol chemical speciation monitor (TOF-ACSM). The receptor site is geographically located in the middle part of China, at the junction of the BTH region and the GZB region, which are two of the three key regions in China's Blue Sky Campaign for pollution control and sustainable development in 2018. In addition, the chemical composition of non-refractory $PM_{2.5}$ (organics, sulfate, nitrate, ammonium and chloride) and OA source apportionment was resolved and analyzed with measured black carbon, gas-phase pollutants (SO_2, CO, NO_2 and O_3) and meteorological parameters to provide complementary mass-based characterization of the transported aerosols.

2 Experimental

2.1 Sampling site and instrumentation

The sampling was carried out on the rooftop of the Le Méridien hotel, which was a 33-floor-tall building, about 200 m above the ground (34.34° N, 109.02° E), during summer from 19 May to 18 June 2018. It is located in the central area of Chan-ba Ecological District (CBE, 129 km^2), which was a new ecological district, located at the eastern part of the GZB region. The sampling site was surrounded by wetlands and lawns.

A TOF-ACSM (Aerodyne Research Inc., Billerica, MA) was deployed in an air-conditioned room on the top floor (32nd) of the Le Méridien hotel for continuous online measurements of non-refractory $PM_{2.5}$ species including organics (Org), sulfate (SO_4^{2-}), nitrate (NO_3^-), ammonium (NH_4^+) and chloride (Cl^-). The sampling time resolution was 5 min. Also, a scanning mobility particle sizer, a differential mobility analyzer (DMA, model 3080) and a condensation particle counter (CPC, model 3772) (TSI Incorporated, Shoreview, Minnesota, USA) were combined for the particle number size distribution measurement between 10–840 nm, which shared an inlet with the TOF-ACSM through a $PM_{2.5}$ cyclone (URG-2000-30ED, URG Corp., Chapel Hill, NC). Black carbon concentration was measured by an Aethalometer (AE33, Magee Scientific) through an individual $PM_{2.5}$ cyclone (SCC, BGI) inlet. The sampling time resolution was 1 min at a flow rate of 5 L min^{-1}. Gas-phase pollutants (SO_2, CO, NO, NO_2 and O_3) were measured by the gas analyzers (Thermo Scientific Inc.). Meteorological data (temperature, RH, wind speed and wind direction) were measured by an

automatic weather station (MAWS201, Vaisala, Vantaa, Finland) and a wind sensor (Vaisala model QMW101-M2). All ambient inlets of instruments were set on the rooftop (33rd, 200 m) and were 1.5 m in height.

2.2 TOF-ACSM operation

The TOF-ACSM has been detailed previously (Fröhlich et al., 2013). Briefly, ambient air was sampled through a $PM_{2.5}$ cyclone and a 9.5 millimeter polished stainless-steel tube (Swagelok company, Solon, OH) with a constant flow rate of 3 L min^{-1} (0.3 L min^{-1} for SMPS and CPC, 0.08 L min^{-1} for TOF-ACSM and 2.62 L min^{-1} for an extra constant flow air pump) for the coarse particles. Following that, particles were focused into a narrow particle beam via a $PM_{2.5}$ aerodynamic lens. Then the particles were evaporated by a thermal standard vaporizer ($\sim$ 600 °C) and ionized by an electron impact ionizer (70 eV), and the resulting ion fragments were analyzed and determined by a time-of-flight mass spectrometer. Also, a Nafion dryer was used to remove moisture prior to entering the TOF-ACSM and SMPS, which kept the relative humidity (RH) of the particle beam under 30 %. Meanwhile, an automatically switching valve was installed on the main air path between the Nafion dryer and TOF-ACSM, which was set to change the sampling flow to a high-efficiency particulate air filter for the detection limit measurement during the acquisition.

Ionization efficiency (IE) and relative ionization efficiency (RIE) calibrations were performed about every $\sim$ 10 d during the campaign. Briefly, pure ammonium nitrate and ammonium sulfate particles were successively atomized by a TSI 3076 atomizer (TSI Incorporated, Shoreview, Minnesota, USA). After that, they were dried by a hollow silica gel drying tube before being imported into SMPS for 300 nm size selection, and then they were counted and measured by the CPC and TOF-ACSM simultaneously. The other parameter calibrations, such as the mass, the baseline and the single ions, were conducted every 3 d.

2.3 Data analysis

The chemical compositions and mass concentrations of $PM_{2.5}$ were analyzed by Tofware (v2.5.13, Tofwerk AG). Organics, nitrate and chloride were analyzed with RIEs of 1.4, 1.1 and 1.3, respectively (Canagaratna et al., 2007). RIEs of ammonium and sulfate were estimated from the averaged results of IE and RIE calibration (4.7 for RIE of ammonium; 0.67 for RIE of sulfate). In addition, a particle collection efficiency (CE) for particle bounce losses was calculated as a value of 0.5, with a slight adjustment of CE value based on a composition-dependent collection efficiency (CDCE) approach following Middlebrook et al. (2012). The resulting mass concentrations of chemicals of $PM_{2.5}$ were well correlated with the mass concentrations of water-soluble inorganic aerosol from our in situ gas and aerosol composition monitor (IGAC, S-611, MachineShop) measurement (Fig. S2 in the Supplement), suggesting the reliability of the TOF-ACSM result analysis.

The OA source apportionment was performed by positive matrix factorization (PMF, Paatero and Tapper, 1994; Paatero, 1997) and a multilinear engine (ME-2, Paatero, 1999). Organic aerosol matrices (data matrix, error matrix, minimum values, time series and m/z from 12–120 atomic mass units in our case) were exported from Tofware and were resolved for source apportionment in PMF-ME-2 Toolkit SoFi (version 6.3, Canonaco et al., 2013). The optimal factor-selection and constraining strategies of SoFi were described by Elser et al. (2016). The details are presented in Sect. S1 in the Supplement.

2.4 Trajectory analysis

The trajectory analysis was performed using the HYSPLIT model (Draxler and Hess, 1998) in Hybrid Single-Particle Lagrangian Integrated Trajectory (HYSPLIT_4). Briefly, trajectories were calculated every 1 h from the air mass data which were downloaded from the National Oceanic and Atmospheric Administration (NOAA, ftp://arlftp.arlhq.noaa.gov/pub/archives/gdas1, last access: 1 March 2019) with 48 h backward trajectories at a height of 200 m. The trajectories were further clustered using TrajStat (TrajStat_v1.2).

2.5 Sulfur oxidation ratio and nitrate oxidation ratio

The sulfur oxidation ratio (SOR) and nitrate oxidation ratio (NOR) are the ratios of sulfate and nitrate to their gaseous precursors, which were widely used to represent the degree of gas-to-particle conversions of sulfur and nitrogen. SOR and NOR are calculated by solving Eqs. (1) and (2) (Ji et al., 2018; Chang et al., 2020).

$$\mathrm{SOR} = n\left[\mathrm{SO_4^{2-}}\right] / \left(n\left[\mathrm{SO_4^{2-}}\right] + n\left[\mathrm{SO_2}\right]\right) \quad (1)$$

$$\mathrm{NOR} = n\left[\mathrm{NO_3^-}\right] / \left(n\left[\mathrm{NO_3^-}\right] + n\left[\mathrm{NO_2}\right]\right) \quad (2)$$

3 Results and discussion

3.1 Overview of the chemical composition, OA sources and regional transport at the receptor site

The observational site with an altitude of $\sim$ 200 m above the ground provides an ideal opportunity to investigate the impact of regional transport on aerosol properties. Figure 1 shows an overview of the time series of the chemical components of NR-$PM_{2.5}$ (organics, sulfate, nitrate, ammonium and chloride), together with meteorological parameters and gas-phase pollutants (SO_2, CO, NO_2 and O_3). The average mass concentration of NR-$PM_{2.5}$ was 21.5 ± 14.9 µg m^{-3}, similar to the previous AMS-ACSM results in western China (24.5 µg m^{-3}; Xu et al., 2014) and southeastern China during summer (14.5–32.9 µg m^{-3}; Huang et al., 2012; Lee et

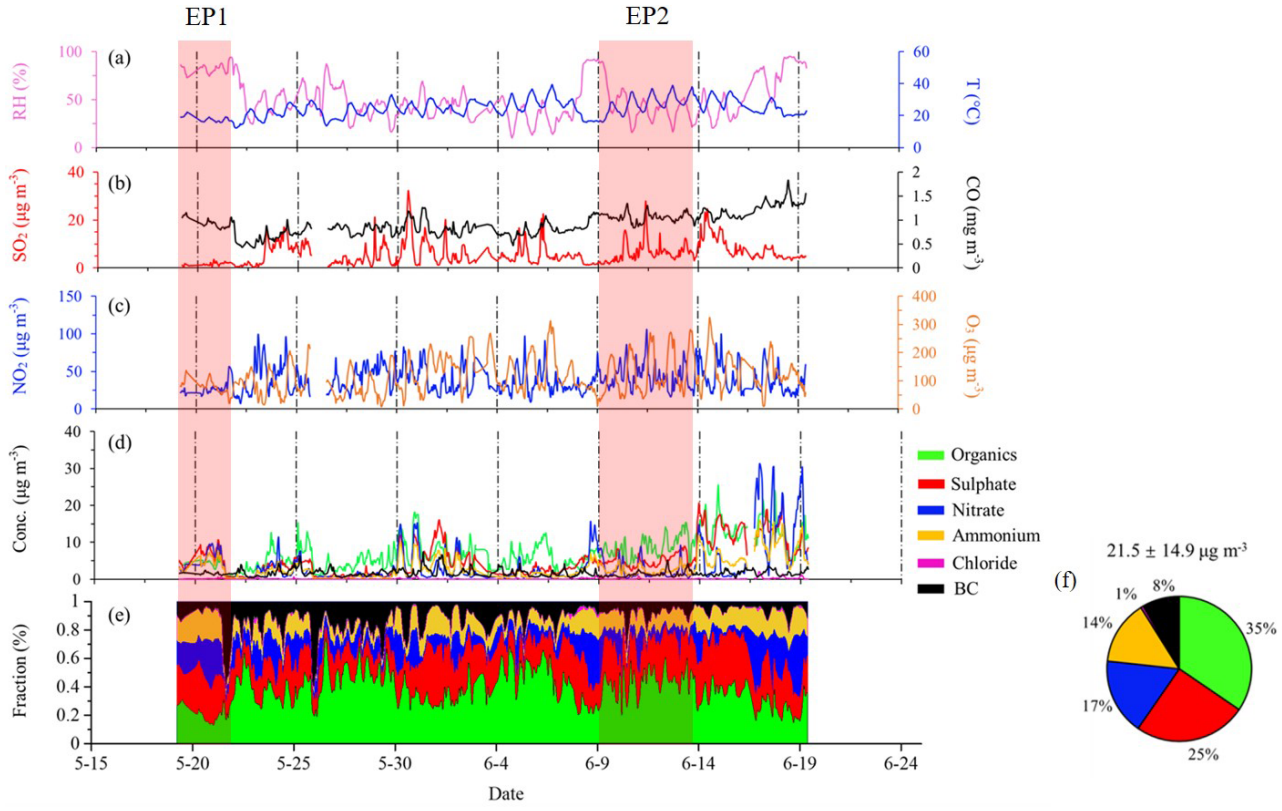

Figure 1. Time series of **(a)** relative humidity and temperature; **(b, c)** mass concentration of SO_2, CO, NO_2 and O_3; and **(d, e)** mass concentrations and fractional contributions of $PM_{2.5}$ (organics, sulfate, nitrate, ammonium, chloride and BC) during the campaign period. Five pollution episodes are observed during the entire campaign, and they are analyzed in detail by the HYSPLIT model and shown in Fig. S3. EP1 and EP2 (shaded) are the only two pollution episodes caused by continuous transport from BTH and urban GZB, respectively. Therefore, they are selected for further discussion.

al., 2013; X. Huang et al., 2013) but was lower than that in northern China (41–80 $\mu g\,m^{-3}$; Hu et al., 2013; Duan et al., 2020). Organics constituted the largest fraction of NR-$PM_{2.5}$ (35 % or 7.5 $\mu g\,m^{-3}$), followed by sulfate (25 % or 5.3 $\mu g\,m^{-3}$), nitrate (17.0 % or 3.7 $\mu g\,m^{-3}$), ammonium (14 % or 3.0 $\mu g\,m^{-3}$), BC (8 % or 1.7 $\mu g\,m^{-3}$) and chloride (1 %, 0.2 $\mu g\,m^{-3}$).

Figure 2 shows the results of wind field maps, cluster-averaged backward trajectories and winds rose analyses. Four transport sectors were identified, including the Beijing–Tianjin–Hebei region (BTH, the east cluster, red), northern China (the north cluster, magenta), the rural Guanzhong Basin region (GZB, the south cluster, green) and the urban GZB region (the west cluster, blue).

BTH transport was characterized by long-distance air mass trajectories advected over the North China Plain with an average wind speed of $1.9 \pm 1.8\,m\,s^{-1}$. The BTH transport sector accounted for 7 % of the total observation days. It showed the highest mass concentration of $PM_{2.5}$ ($32.9 \pm 17.4\,\mu g\,m^{-3}$).

The northern China transport sector was clustered by transport from Mongolia and the northern part of China, including Inner Mongolia and northern Shaanxi Province. It represented the longest transport distance with an average wind speed of $2.2 \pm 2.1\,m\,s^{-1}$ and accounted for 22 % of observation days. The $PM_{2.5}$ mass in the northern China transport sector was $24.9 \pm 12.9\,\mu g\,m^{-3}$, which was lower than that in the BTH transport sector.

The urban GZB transport sector was from the west of the GZB region, including large cities in the GZB region, such as Baoji, Xianyang and Xi'an. The urban GZB transport sector was the most frequent pathway during the campaign, accounting for 60 % of observation days with an average wind speed of $1.0 \pm 0.9\,m\,s^{-1}$. The $PM_{2.5}$ mass in the urban GZB transport sector was $21.7 \pm 14.8\,\mu g\,m^{-3}$. Finally, the rural GZB transport sector mainly consisted of air masses from Mt. Qinling, representing the air mass with the least anthropogenic influence and accounting for 11 % of observation days with an average wind speed of $1.9 \pm 0.7\,m\,s^{-1}$ and the lowest average $PM_{2.5}$ mass ($8.8 \pm 5.5\,\mu g\,m^{-3}$).

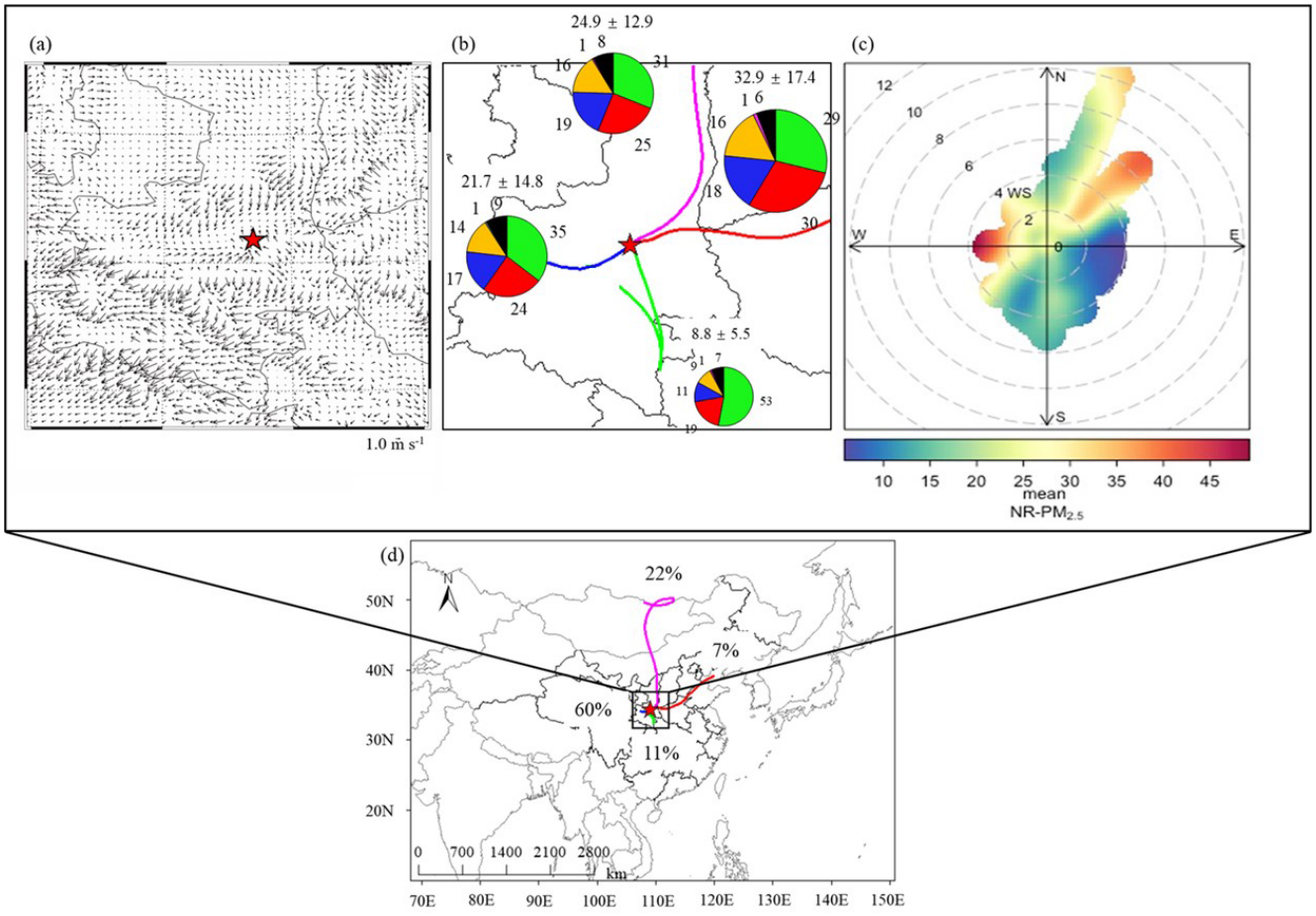

Figure 2. **(a)** Wind field, **(b, d)** backward trajectory and **(c)** wind rose results during the campaign. There are four transport clusters observed during the campaign, which are northern China transport (the north cluster, magenta, 22 % of observation days) and BTH transport (the east cluster, red, 7 % of observation days), western GZB transport (the west cluster, blue, 60 % of observation days) and southern GZB transport (the south cluster, green, 11 % of observation days).

3.2 Secondary inorganic formation during the transport

Figure 3 shows the mass concentrations of the measured components, their fractional contributions, the sulfur oxidation ratio (SOR) and the nitrogen oxidation ratio (NOR) in these four transport sectors. SIA showed the highest mass concentration of $21.4 \pm 11.9\,\mu g\,m^{-3}$ in the BTH transport sector, followed by the northern China transport sector ($15.2 \pm 6.6\,\mu g\,m^{-3}$), the urban GZB transport sector ($12.2 \pm 3.1\,\mu g\,m^{-3}$) and the rural GZB transport sector ($3.5 \pm 1.7\,\mu g\,m^{-3}$). The corresponding fractional contributions of SIA to $PM_{2.5}$ were 64 %, 60 %, 55 % and 39 %. The difference in SIA mass and fractional contributions suggests the difference in SIA precursor concentrations (i.e., SO_2, NO_x and NH_3) and SIA formation efficiency among different transport sectors, as discussed below.

Sulfate was the dominant fraction in the BTH transport sector, accounting for 30 % of $PM_{2.5}$. This fraction decreased to 25 % and 24 % in the northern China transport sector and the urban GZB transport sector, respectively. Nitrate showed no obvious difference in the three urban transport sectors, accounting for 17 %–19 % of $PM_{2.5}$. For the rural GZB transport sector, the fraction of sulfate and nitrate largely decreased to 19 % and 11 % of $PM_{2.5}$, respectively, consistent with lower SO_2 ($3.2 \pm 2.5\,\mu g\,m^{-3}$) and NO_2 ($27.8 \pm 10.3\,\mu g\,m^{-3}$) in the rural GZB transport sector, which was about half of that in the three urban transport sectors (6.3–7.3 $\mu g\,m^{-3}$ for SO_2 and 44.7–51.3 $\mu g\,m^{-3}$ for NO_2). The high fraction of sulfate in the BTH transport sector was supported by high concentrations of SO_2 and sulfate in the BTH region and central China region (Du et al., 2019; Chen et al., 2020; Li et al., 2021a; Sun et al., 2022). It was further supported by high sulfur conversion efficiency (SOR), for which the BTH transport sector showed the highest SOR of 0.58, followed by the northern China transport sector (0.52), the urban GZB transport sector (0.49) and the rural GZB transport sector (0.44) (Fig. 3c). Similarly, NOR showed a relatively high value of 0.29 in the BTH transport sector and the northern China transport sector and was

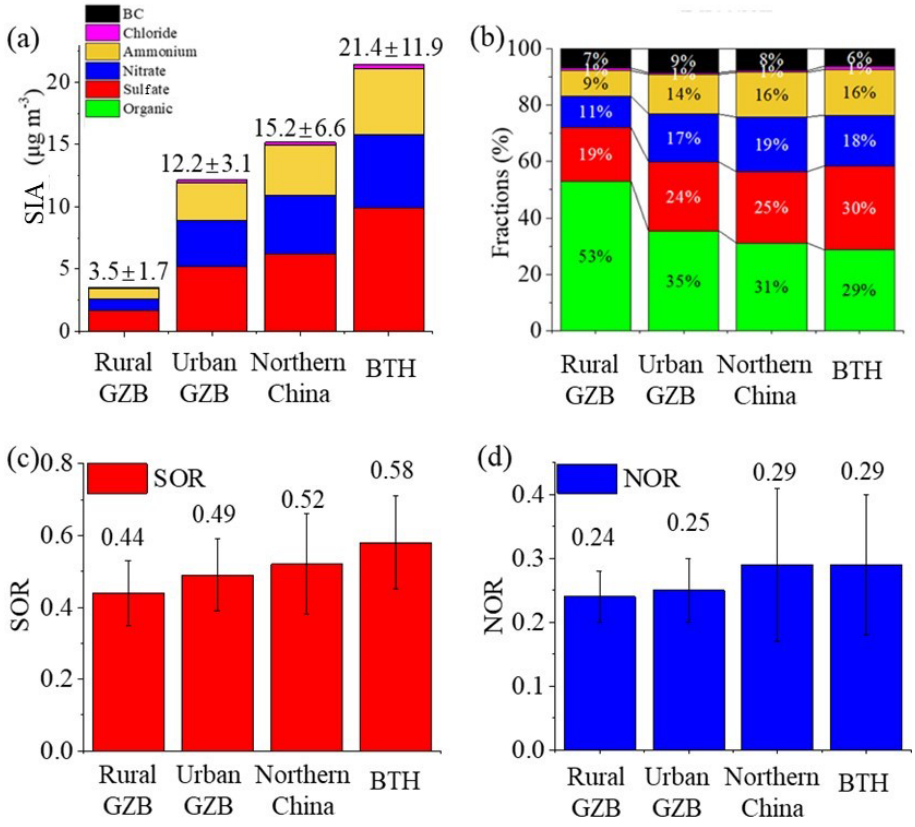

Figure 3. The comparison of **(a)** the mass concentration of SIA, **(b)** chemical fractions of $PM_{2.5}$, **(c)** sulfur oxidation ratio (SOR) and **(d)** nitrogen oxidation ratio (NOR) in the four transport sectors.

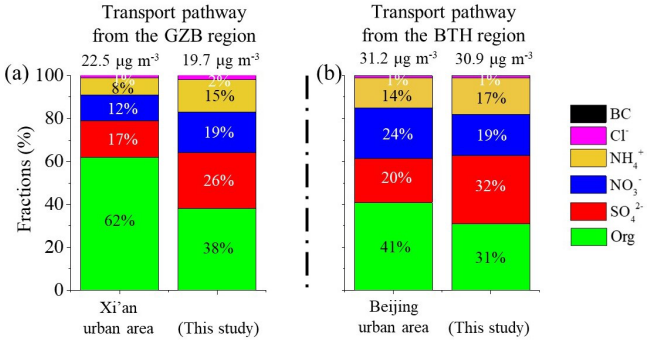

Figure 4. Chemical composition of the observation results which were long-term and right on the transport route of the BTH transport and the GZB transport, including the Beijing urban area (Xu et al., 2019), the Xi'an urban area (Duan et al., 2021), the BTH transport in this study (east transport) and the urban GZB transport in this study (west transport).

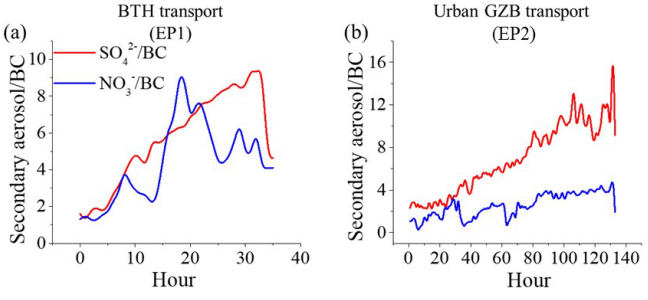

Figure 5. The relationship between production of the secondary inorganic aerosol and transport duration in the pollution episodes. EP1 and EP2 represented the pollution episodes caused by the BTH transport and the urban GZB transport, respectively.

slightly low in the urban GZB transport sector (0.25) and the rural GZB transport sector (0.24), consistent with the high nitrate fraction in the BTH transport sector and the northern China sector (Fig. 3d). In comparison with the previously reported results, which were investigated in the source regions of the urban GZB transport sector and the BTH transport sector (Xu et al., 2019; Duan et al., 2021), SOR and NOR showed an obvious increase after transport. For SOR it increased from 0.36 to 0.44 in the urban GZB transport pathway and from 0.53 to 0.58 in the BTH transport pathway, while for NOR it increased from 0.06 to 0.25 in the urban GZB transport pathway and from 0.15 to 0.29 in the BTH transport pathway. The increases in SOR and NOR after

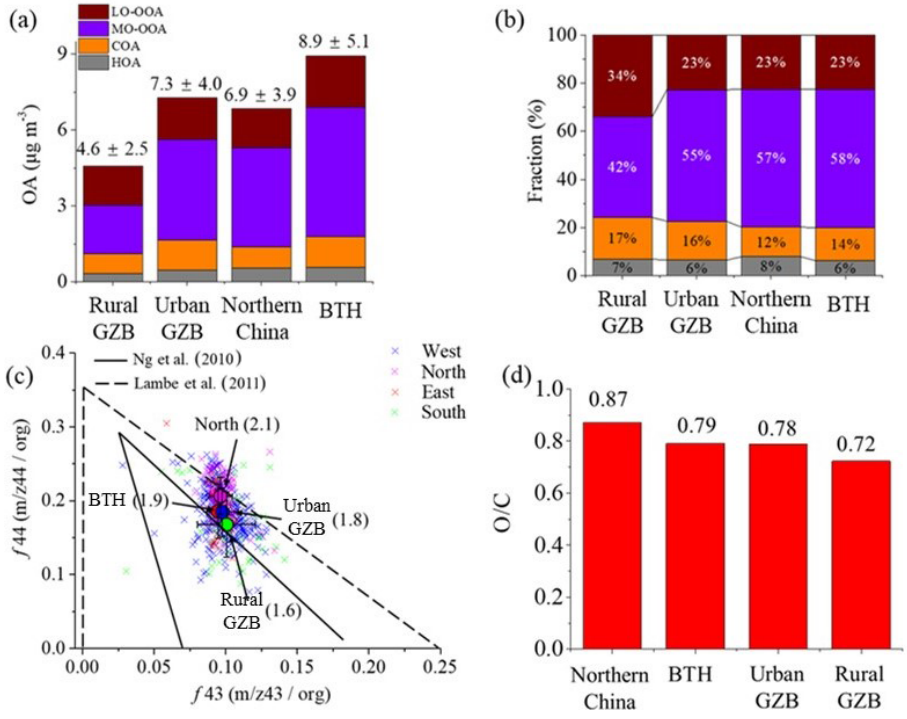

Figure 6. The comparison of **(a)** the mass concentration and **(b)** fractions of organic aerosol. **(c)** Scatter plot of f_{44} vs. f_{43} in four transport directions. The triangles from Ng et al. (2010) and Lambe et al. (2011) are drawn as a solid line and a dotted line, respectively. **(d)** The O / C ratio in four transport directions.

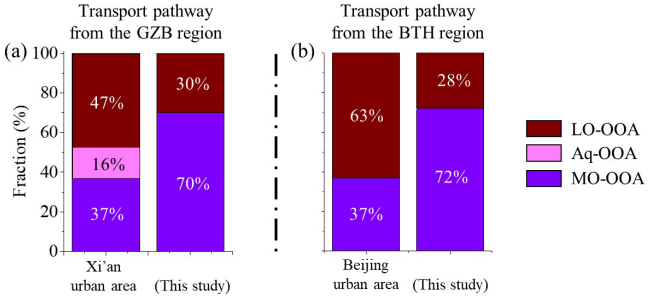

Figure 7. OA factors of the observation results which were long-term and were right on the transport route of the BTH transport and the GZB transport, including the Beijing urban area (Xu et al., 2019), the Xi'an urban area (Duan et al., 2021), the BTH transport in this study (east transport) and the urban GZB transport in this study (west transport).

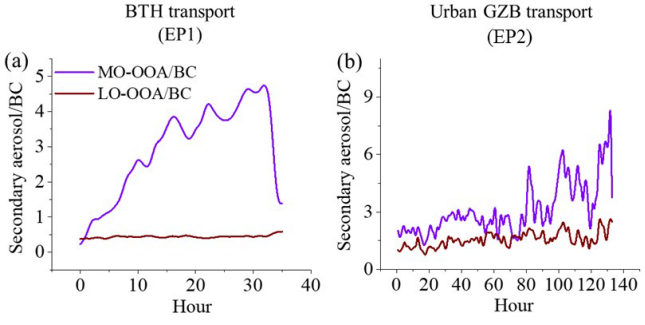

Figure 8. The relationship between production of the secondary organic aerosol and transport duration in the pollution episodes. EP1 and EP2 represented the pollution episodes caused by the BTH transport and the urban GZB transport, respectively.

transport suggest efficient sulfate and nitrate formation during regional transport. This was also reflected in the sulfate and nitrate fractions (Fig. 4). After transport, the fractional contribution of sulfate increased from 17 % (3.8 μg m^{-3}) to 26 % (5.6 μg m^{-3}) in the urban GZB transport pathway and from 20 % (6.2 μg m^{-3}) to 32 % (9.9 μg m^{-3}) in the BTH transport pathway, while the nitrate fraction increased from 12 % (2.7 μg m^{-3}) to 19 % (3.7 μg m^{-3}) in the urban GZB transport pathway but slightly decreased from 24 % (7.4 μg m^{-3}) to 19 % (5.9 μg m^{-3}) in the BTH transport pathway likely due to the mass loss of semi-volatile aerosol species (such as NH_4NO_3) when aerosols are exposed to a cleaner environment during long-distance transport (Liu et al., 2021). We also compared the pollution episodes caused by the continuous transport from the BTH (EP1) and the urban GZB (EP2) (as shown in the shaded area in Fig. 1, detailed in Fig. S3). Sulfate and nitrate were normalized by BC to minimize the influence of primary emission or dilution (Fig. 5). The sulfate / BC ratio increased with transport

in both EP1 and EP2, with a growth rate of $0.26\,h^{-1}$ during EP1 (increased from 1.2 to 9.4 in 31 h) and of $0.1\,h^{-1}$ during EP2 (increased from 2.3 to 16.2 in 131 h). The nitrate / BC ratio showed a growth rate of $0.17\,h^{-1}$ during EP1 (increased from 1.3 to 6.6 in 31 h) and of 5.7 times lower during EP2 ($0.03\,h^{-1}$, increased from 1.1 to 4.7 in 131 h). The comparison of these two episodes further supports stronger formation of SIA in the BTH transport sector. The difference in the formation efficiency of sulfate and nitrate in different transport air masses may be related to RH, because aqueous-phase oxidation was an important formation pathway for sulfate in high-RH conditions (Cheng et al., 2016; Xue et al., 2019; Chang et al., 2020), and high RH also strengthened the conversion of gas-phase NH_4NO_3 to the particle phase (Huang et al., 2020), which likely leads to high SOR and NOR in the BTH transport sector (81 ± 17 % of average RH).

3.3 Secondary organic formation during transport

Figure 6 shows the mass concentrations of the resolved OA factors, their fractional contributions, the f_{44}-to-f_{43} ratio and O / C ratio in these four transport sectors. The f_{44} / f_{43} ratio and O / C ratio are important indicators of the oxidation state of bulk OA (Ng et al., 2010) that were widely used in previous studies for SOA oxidation analysis (Xu et al., 2014; Canonaco et al., 2015; Reyes-Villegas et al., 2016). The BTH transport sector showed the highest OA mass concentration of $8.9 \pm 5.1\,\mu g\,m^{-3}$, followed by the urban GZB transport sector ($7.3 \pm 4.0\,\mu g\,m^{-3}$), the northern China transport sector ($6.9 \pm 3.9\,\mu g\,m^{-3}$) and the rural GZB transport sector ($4.6 \pm 2.5\,\mu g\,m^{-3}$). The corresponding fractional contributions of MO-OOA to total OA were 58 % ($5.2\,\mu g\,m^{-3}$), 55 % ($4.0\,\mu g\,m^{-3}$), 57 % ($4.0\,\mu g\,m^{-3}$) and 42 % ($1.9\,\mu g\,m^{-3}$), constituting the major OA source in the four transport sectors. The LO-OOA fraction was higher in the rural GZB transport sector (34 %, $1.9\,\mu g\,m^{-3}$) compared to the other three urban transport sectors (around 23 %, 3.9–5.2 $\mu g\,m^{-3}$), suggesting that SOA was less oxidized in the rural transport sector. The northern China transport sector showed the highest f_{44} / f_{43} ratio of 2.1 and O / C ratio of 0.87, followed by the BTH transport sector (1.9 and 0.78), the urban GZB transport sector (1.8 and 0.72) and much lower values in the rural GZB transport sector (1.6 and 0.58). The higher f_{44} / f_{43} and O / C ratios in the northern China transport sector and the BTH transport sector suggest sufficient OA aging during long-range transport. The f_{44} / f_{43} ratios in these four transport sectors were higher than those in the urban sites in previous studies (triangle in Fig. 6c, Ng et al., 2011), and the O / C ratios in these four transport sectors (0.72–0.87) were also much higher than those measured in urban sites in China during summer, such as Lanzhou (0.33; Xu et al., 2014) and Jiaxing (0.28; X. Huang et al., 2013), but similar to the results from the mountainous site in the North China Plain during summer (0.75; Li et al., 2021a) and the long-range transport study in the United States (0.8; Gunsch et al., 2018). Note that the O / C ratios in the transport sectors were also much higher than those measured in the source regions of the urban GZB transport sector and the BTH transport sector, with the O / C ratio increasing from 0.54 to 0.78 in the BTH transport pathway and from 0.58 to 0.72 in the urban GZB transport pathway after transport. The corresponding MO-OOA to SOA fraction also increased from 37 % ($3.4\,\mu g\,m^{-3}$) to 72 % ($5.2\,\mu g\,m^{-3}$) in the BTH transport pathway and from 37 % ($3.6\,\mu g\,m^{-3}$) to 70 % ($4.0\,\mu g\,m^{-3}$) in the urban GZB transport pathway (Fig. 7), suggesting regional transport enhanced the OA aging process and thus the OA oxidation state. The growth rates of MO-OOA and LO-OOA during the pollution episodes of EP1 and EP2 are shown in Fig. 8. Similar to SIA, the MO-OOA / BC ratio increased with the transport duration for both episodes. It showed a growth rate of $0.15\,h^{-1}$ during EP1 (increased from 0.23 to 4.77 in 31 h) and of $0.06\,h^{-1}$ during EP2 (increased from 1.58 to 9.59 in 131 h), suggesting stronger formation of MO-OOA in the BTH transport sector. Conversely, LO-OOA showed no obvious increasing trend with the transport duration during EP1 and EP2, likely due to a higher conversion efficiency from LO-OOA to MO-OOA.

4 Conclusion

The observation at ~ 200 m above the ground at the junction of the North China Plain and Fenwei Basin showed that the fraction of SIA and MO-OOA increased significantly after transport. The sulfur oxidation rate (SOR, 0.49–0.58), nitrogen oxidation rate (NOR, 0.25–0.29), f_{44} / f_{43} ratio (1.6–2.1) and O / C ratio (0.72–0.87) were significantly higher than those investigated locally, indicating that long-distance transport largely enhanced the SIA formation, the OA oxidation and aging. The formation rate of sulfate, nitrate and MO-OOA in the BTH transport sector was much higher than that in the GZB transport sector, indicating the stronger sulfate, nitrate and MO-OOA formation efficiency in the BTH transport sector.

Data availability. The detailed data can be obtained from https://doi.org/10.5281/zenodo.6446514 (Zhong, 2022).

Supplement. The supplement related to this article is available online at: https://doi.org/10.5194/acp-22-9513-2022-supplement.

Author contributions. RJH designed the study. Data analysis was done by HBZ and RJH. HBZ and RJH wrote the manuscript. HBZ and RJH interpreted data and prepared display items. All authors commented on and discussed the manuscript.

Competing interests. The contact author has declared that none of the authors has any competing interests.

Disclaimer. Publisher's note: Copernicus Publications remains neutral with regard to jurisdictional claims in published maps and institutional affiliations.

Acknowledgements. The authors acknowledge support from the National Natural Science Foundation of China (NSFC) under grant nos. 41925015 and 41877408, the Key Research Program of Frontier Sciences from the Chinese Academy of Sciences (no. ZDBS-LY-DQC001), the Strategic Priority Research Program of the Chinese Academy of Sciences (no. XDB40000000), and SKLLQG (no. SKLLQGTD1801).

Financial support. This work was financial supported by the National Natural Science Foundation of China (NSFC) under grant nos. 41925015 and 41877408, the Key Research Program of Frontier Sciences from the Chinese Academy of Sciences (no. ZDBS-LY-DQC001), the Strategic Priority Research Program of the Chinese Academy of Sciences (no. XDB40000000), and SKLLQG (no. SKLLQGTD1801).

Review statement. This paper was edited by Dantong Liu and reviewed by two anonymous referees.

References

An, Z., Huang, R., Zhang, R., Tie, X., Li, G., Cao, J., Zhou, W., Shi, Z., Han, Y., Gu, Z., and Ji, Y.: Severe haze in northern China: A synergy of anthropogenic emissions and atmospheric processes, P. Natl. Acad. Sci. USA, 116, 8657–8666, 2019.

Braun, R. A., Aghdam, M. A., Bañaga, P. A., Betito, G., Cambaliza, M. O., Cruz, M. T., Lorenzo, G. R., MacDonald, A. B., Simpas, J. B., Stahl, C., and Sorooshian, A.: Long-range aerosol transport and impacts on size-resolved aerosol composition in Metro Manila, Philippines, Atmos. Chem. Phys., 20, 2387–2405, https://doi.org/10.5194/acp-20-2387-2020, 2020.

Calvo, A., Alves, C., Castro, A., Pont, V., Vicente, A., and Fraile, R.: Research on aerosol sources and chemical composition: past, current and emerging issues, Atmos. Res., 120, 1–28, 2013.

Canagaratna, M., Jayne, J., Jimenez, J., Allan, J., Alfarra, M., Zhang, Q., Onasch, T., Drewnick, F., Coe, H., Middlebrook, A., Delia, A., Williams, L., Trimborn, A., Northway, M., DeCarlo, P., Kolb, C., Davidovits, P., and Worsnop, D.: Chemical and microphysical characterization of ambient aerosols with the Aerodyne aerosol mass spectrometer, Mass Spectrom. Rev., 26, 185–222, 2007.

Canonaco, F., Crippa, M., Slowik, J. G., Baltensperger, U., and Prévôt, A. S. H.: SoFi, an IGOR-based interface for the efficient use of the generalized multilinear engine (ME-2) for the source apportionment: ME-2 application to aerosol mass spectrometer data, Atmos. Meas. Tech., 6, 3649–3661, https://doi.org/10.5194/amt-6-3649-2013, 2013.

Canonaco, F., Slowik, J. G., Baltensperger, U., and Prévôt, A. S. H.: Seasonal differences in oxygenated organic aerosol composition: implications for emissions sources and factor analysis, Atmos. Chem. Phys., 15, 6993–7002, https://doi.org/10.5194/acp-15-6993-2015, 2015.

Cao, J., Wang, Q., Chow, J., Watson, J., Tie, X., Shen, Z., Wang, P., and An, Z.: Impacts of aerosol compositions on visibility impairment in Xi'an, China, Atmos. Environ., 59, 559–566, 2012.

Chang, Y., Huang, R.-J., Ge, X., Huang, X., Hu, J., Duan, Y., Zou, Z., Liu, X., and Lehmann, M. F.: Puzzling haze events in China during the coronavirus (COVID-19) shutdown, Geophys. Res. Lett., 47, e2020GL088533, https://doi.org/10.1029/2020GL088533, 2020.

Chen, T., Liu, J., Liu, Y., Ma, Q., Ge, Y., Zhong, C., Jiang, H., Chu, B., Zhang, P., Ma, J., Liu, P., Wang, Y., Mu, Y., and He, H.: Chemical characterization of submicron aerosol in summertime Beijing: A case study in southern suburbs in 2018, Chemosphere, 247, 125918, https://doi.org/10.1016/j.chemosphere.2020.125918, 2020.

Chen, W., Ye, Y., Hu, W., Zhou, H., Pan, T., Wang, Y., Song, W., Song, Q., Ye, C., Wang, C., Wang, B., Huang, S., Yuan, B., Zhu, M., Lian, X., Zhang, G., Bi, X., Jiang, F., Liu, J., Canonaco, F., Prévôt, A., Shao, M., and Wang, X.: Real-time characterization of aerosol compositions, sources, and aging processes in Guangzhou during PRIDE-GBA 2018 campaign, J. Geophys. Res.-Atmos., 126, e2021JD035114, https://doi.org/10.1029/2021JD035114, 2021.

Cheng, Y., Zheng, G., Wei, C., Mu, Q., Zheng, B., Wang, Z., Gao, M., Zhang, Q., He, K., Carmichael, G., Poschl, U., and Su, H.: Reactive nitrogen chemistry in aerosol water as a source of sulfate during haze events in China, Sci. Adv., 2, e1601530, https://doi.org/10.1126/sciadv.1601530, 2016.

Cohen, A., Brauer, M., Burnett, R., Anderson, H., Frostad, J., Estep, K., Balakrishnan, K., Brunekreef, B., Dandona, L., Dandona, R., Feigin, V., Freedman, G., Hubbell, B., Jobling, A., Kan, H., Knibbs, L., Liu, Y., Martin, R., Morawska, L., Pope III, C., Shin, H., Straif, K., Shaddick, G., Thomas, M., van Dingenen, R., van Donkelaar, A., Vos, T., Murray, C., and Forouzanfar, M.: Estimates and 25-year trends of the global burden of disease attributable to ambient air pollution: an analysis of data from the Global Burden of Diseases Study 2015, Lancet, 389, 1907–1918, 2017.

Das, S. and Jayaraman, A.: Long-range transportation of anthropogenic aerosols over eastern coastal region of India: investigation of sources and impact on regional climate change, Atmos. Res., 118, 68–83, 2012.

Draxler, R. R. and Hess, G. D.: An overview of the HYSPLIT_4 modelling system for trajectories, dispersion, and deposition, Aust. Meteorol. Mag., 47, 295–308, 1998.

Du, H., Li, J., Chen, X., Wang, Z., Sun, Y., Fu, P., Li, J., Gao, J., and Wei, Y.: Modeling of aerosol property evolution during winter haze episodes over a megacity cluster in northern China: roles of regional transport and heterogeneous reactions of SO_2, Atmos. Chem. Phys., 19, 9351–9370, https://doi.org/10.5194/acp-19-9351-2019, 2019.

Duan, J., Huang, R.-J., Li, Y., Chen, Q., Zheng, Y., Chen, Y., Lin, C., Ni, H., Wang, M., Ovadnevaite, J., Ceburnis, D., Chen, C., Worsnop, D. R., Hoffmann, T., O'Dowd, C., and Cao, J.: Summertime and wintertime atmospheric processes of sec-

ondary aerosol in Beijing, Atmos. Chem. Phys., 20, 3793–3807, https://doi.org/10.5194/acp-20-3793-2020, 2020.

Duan, J., Huang, R.-J., Gu, Y., Lin, C., Zhong, H., Wang, Y., Yuan W., Ni, H., Yang, L., Chen, Y., Worsnop, D., and O'Dowd, C.: The formation and evolution of secondary organic aerosol during summer in Xi'an: Aqueous phase processing in fog-rain days, Sci. Total Environ., 756, 144077, https://doi.org/10.1016/j.scitotenv.2020.144077, 2021.

Elser, M., Huang, R.-J., Wolf, R., Slowik, J. G., Wang, Q., Canonaco, F., Li, G., Bozzetti, C., Daellenbach, K. R., Huang, Y., Zhang, R., Li, Z., Cao, J., Baltensperger, U., El-Haddad, I., and Prévôt, A. S. H.: New insights into $PM_{2.5}$ chemical composition and sources in two major cities in China during extreme haze events using aerosol mass spectrometry, Atmos. Chem. Phys., 16, 3207–3225, https://doi.org/10.5194/acp-16-3207-2016, 2016.

Feng, T., Bei, N., Zhao, S., Wu, J., Li, X., Zhang, T., Cao, J., Zhou, W., and Li, G.: Wintertime nitrate formation during haze days in the Guanzhong basin, China: a case study, Environ. Pollut., 243, 1057–1067, 2018.

Fierce, L., Bond, T. C., Bauer, S. E., Mena, F., and Riemer, N.: Black carbon absorption at the global scale is affected by particle-scale diversity in composition, Nat. Commun., 7, 12361, https://doi.org/10.1038/ncomms12361, 2016.

Fröhlich, R., Cubison, M. J., Slowik, J. G., Bukowiecki, N., Prévôt, A. S. H., Baltensperger, U., Schneider, J., Kimmel, J. R., Gonin, M., Rohner, U., Worsnop, D. R., and Jayne, J. T.: The ToF-ACSM: a portable aerosol chemical speciation monitor with TOFMS detection, Atmos. Meas. Tech., 6, 3225–3241, https://doi.org/10.5194/amt-6-3225-2013, 2013.

Gunsch, M. J., May, N. W., Wen, M., Bottenus, C. L. H., Gardner, D. J., VanReken, T. M., Bertman, S. B., Hopke, P. K., Ault, A. P., and Pratt, K. A.: Ubiquitous influence of wildfire emissions and secondary organic aerosol on summertime atmospheric aerosol in the forested Great Lakes region, Atmos. Chem. Phys., 18, 3701–3715, https://doi.org/10.5194/acp-18-3701-2018, 2018.

Guo, J., Zhou, S., Cai, M., Zhao, J., Song, W., Zhao, W., Hu, W., Sun, Y., He, Y., Yang, C., Xu, X., Zhang, Z., Cheng, P., Fan, Q., Hang, J., Fan, S., Wang, X., and Wang, X.: Characterization of submicron particles by time-of-flight aerosol chemical speciation monitor (ToF-ACSM) during wintertime: aerosol composition, sources, and chemical processes in Guangzhou, China, Atmos. Chem. Phys., 20, 7595–7615, https://doi.org/10.5194/acp-20-7595-2020, 2020.

Hu, W. W., Hu, M., Yuan, B., Jimenez, J. L., Tang, Q., Peng, J. F., Hu, W., Shao, M., Wang, M., Zeng, L. M., Wu, Y. S., Gong, Z. H., Huang, X. F., and He, L. Y.: Insights on organic aerosol aging and the influence of coal combustion at a regional receptor site of central eastern China, Atmos. Chem. Phys., 13, 10095–10112, https://doi.org/10.5194/acp-13-10095-2013, 2013.

Huang, R., Zhang, Y., Bozzetti, C., Ho, K., Cao, J., Han, Y., Daellenbach, K. R., Slowik, J. G., Platt, S. M., and Canonaco, F.: High secondary aerosol contribution to particulate pollution during haze events in China, Nature, 514, 218–222, 2014.

Huang, X., Xue, L., Tian, X., Shao, W., Sun, T., Gong, Z., Ju, W., Jiang, B., Hu, M., and He, L.: Highly time-resolved carbonaceous aerosol characterization in yangtze river delta of china: Composition, mixing state and secondary formation, Atmos. Environ., 64, 200–207, 2013.

Huang, X., Ding, A., Wang, Z., Ding, K., Gao, J., Chai, F., and Fu, C.: Amplified transboundary transport of haze by aerosol–boundary layer interaction in China, Nat. Geosci., 13, 428–434, 2020.

Huang, X.-F., He, L.-Y., Xue, L., Sun, T.-L., Zeng, L.-W., Gong, Z.-H., Hu, M., and Zhu, T.: Highly time-resolved chemical characterization of atmospheric fine particles during 2010 Shanghai World Expo, Atmos. Chem. Phys., 12, 4897–4907, https://doi.org/10.5194/acp-12-4897-2012, 2012.

Huang, Y., Li, L., Li, J., Wang, X., Chen, H., Chen, J., Yang, X., Gross, D. S., Wang, H., Qiao, L., and Chen, C.: A case study of the highly time-resolved evolution of aerosol chemical and optical properties in urban Shanghai, China, Atmos. Chem. Phys., 13, 3931–3944, https://doi.org/10.5194/acp-13-3931-2013, 2013.

Ji, Y., Qin, X., Wang, B., Xu, J., Shen, J., Chen, J., Huang, K., Deng, C., Yan, R., Xu, K., and Zhang, T.: Counteractive effects of regional transport and emission control on the formation of fine particles: a case study during the Hangzhou G20 summit, Atmos. Chem. Phys., 18, 13581–13600, https://doi.org/10.5194/acp-18-13581-2018, 2018.

Lambe, A. T., Onasch, T. B., Massoli, P., Croasdale, D. R., Wright, J. P., Ahern, A. T., Williams, L. R., Worsnop, D. R., Brune, W. H., and Davidovits, P.: Laboratory studies of the chemical composition and cloud condensation nuclei (CCN) activity of secondary organic aerosol (SOA) and oxidized primary organic aerosol (OPOA), Atmos. Chem. Phys., 11, 8913–8928, https://doi.org/10.5194/acp-11-8913-2011, 2011.

Lee, B., Li, Y., Yu, J., Louie, P., and Chan, C.: Physical and chemical characterization of ambient aerosol by HR-ToF-AMS at a suburban site in Hong Kong during springtime 2011, J. Geophys. Res., 118, 8625–8639, 2013.

Lei, Y., Zhang, Q., He, K. B., and Streets, D. G.: Primary anthropogenic aerosol emission trends for China, 1990–2005, Atmos. Chem. Phys., 11, 931–954, https://doi.org/10.5194/acp-11-931-2011, 2011.

Lelieveld, J., Evans, J. S., Fnais, M., Giannadaki, D., and Pozzer, A.: The contribution of outdoor air pollution sources to premature mortality on a global scale, Nature, 525, 367–371, 2015.

Li, H., Cheng, J., Zhang, Q., Zheng, B., Zhang, Y., Zheng, G., and He, K.: Rapid transition in winter aerosol composition in Beijing from 2014 to 2017: response to clean air actions, Atmos. Chem. Phys., 19, 11485–11499, https://doi.org/10.5194/acp-19-11485-2019, 2019.

Li, J. and Han, Z.: A modeling study of severe winter haze events in Beijing and its neighboring regions, Atmos. Res., 170, 87–97, 2016.

Li, J., Du, H., Wang, Z., Sun, Y., Yang, W., Li, J., Tang, X., and Fu, P.: Rapid formation of a severe regional winter haze episode over a mega-city cluster on the North China Plain, Environ. Pollut., 223, 605–615, 2017.

Li, J., Liu, Z., Cao, L., Gao, W., Yan, Y., Mao, J., Zhang, X., He, L., Xin, J., Tang, G., Ji, D., Hu, B., Wang, L., Wang, Y., Dai, L., Zhao, D., Du, W., and Wang, Y.: Highly time-resolved chemical characterization and implications of regional transport for submicron aerosols in the North China Plain, Sci. Total Environ., 705, 135803, https://doi.org/10.1016/j.scitotenv.2019.135803, 2021a.

Li, J., Cao, L., Gao, W., He, L., Yan, Y., He, Y., Pan, Y., Ji, D., Liu, Z., and Wang, Y.: Seasonal variations in the highly time-

resolved aerosol composition, sources and chemical processes of background submicron particles in the North China Plain, Atmos. Chem. Phys., 21, 4521–4539, https://doi.org/10.5194/acp-21-4521-2021, 2021b.

Li, Y. J., Lee, B. P., Su, L., Fung, J. C. H., and Chan, C. K.: Seasonal characteristics of fine particulate matter (PM) based on high-resolution time-of-flight aerosol mass spectrometric (HR-ToF-AMS) measurements at the HKUST Supersite in Hong Kong, Atmos. Chem. Phys., 15, 37–53, https://doi.org/10.5194/acp-15-37-2015, 2015.

Lin, C., Huang, R.-J., Duan, J., Zhong, H., Xu, W., Wu, Y., and Zhang, R.: Large contribution from worship activities to the atmospheric soot particles in northwest China, Environ. Pollut., 299, 118907, https://doi.org/10.1016/j.envpol.2022.118907, 2022.

Liu, Q., Liu, D., Wu, Y., Bi, K., Gao, W., Tian, P., Zhao, D., Li, S., Yu, C., Tang, G., Wu, Y., Hu, K., Ding, S., Gao, Q., Wang, F., Kong, S., He, H., Huang, M., and Ding, D.: Reduced volatility of aerosols from surface emissions to the top of the planetary boundary layer, Atmos. Chem. Phys., 21, 14749–14760, https://doi.org/10.5194/acp-21-14749-2021, 2021.

Liu, Z., Gao, W., Yu, Y., Hu, B., Xin, J., Sun, Y., Wang, L., Wang, G., Bi, X., Zhang, G., Xu, H., Cong, Z., He, J., Xu, J., and Wang, Y.: Characteristics of $PM_{2.5}$ mass concentrations and chemical species in urban and background areas of China: emerging results from the CARE-China network, Atmos. Chem. Phys., 18, 8849–8871, https://doi.org/10.5194/acp-18-8849-2018, 2018.

Middlebrook, A., Bahreini, R., Jimenez, J., and Canagaratna, M.: Evaluation of composition-dependent collection efficiencies for the aerodyne aerosol mass spectrometer using field data, Aerosol Sci. Tech., 46, 258–271, 2012.

Moffet, R. C. and Prather, K. A.: In-situ measurements of the mixing state and optical properties of soot with implications for radiative forcing estimates, P. Natl. Acad. Sci. USA, 106, 11872–11877, 2009.

Ng, N. L., Canagaratna, M. R., Zhang, Q., Jimenez, J. L., Tian, J., Ulbrich, I. M., Kroll, J. H., Docherty, K. S., Chhabra, P. S., Bahreini, R., Murphy, S. M., Seinfeld, J. H., Hildebrandt, L., Donahue, N. M., DeCarlo, P. F., Lanz, V. A., Prévôt, A. S. H., Dinar, E., Rudich, Y., and Worsnop, D. R.: Organic aerosol components observed in Northern Hemispheric datasets from Aerosol Mass Spectrometry, Atmos. Chem. Phys., 10, 4625–4641, https://doi.org/10.5194/acp-10-4625-2010, 2010.

Paatero, P.: Least squares formulation of robust non-negative factor analysis, Chemom. Intell. Lab., 37, 23–35, 1997.

Paatero, P.: The multilinear engine: a table-driven, least squares program for solving multilinear problems, including the n-way parallel factor analysis model, J. Comput. Graph. Stat., 8, 854–888, 1999.

Paatero, P. and Tapper, U.: Positive Matrix Factorization: a nonnegative factor model with optimal utilization of error estimates of data values, Environmetrics, 5, 111–126, 1994.

Pu, W., Zhao, X., Shi, X., Ma, Z., Zhang, X., and Bo, Y.: Impact of long-range transport on aerosol properties at a regional background station in Northern China, Atmos. Res., 153, 489–499, 2015.

Reyes-Villegas, E., Green, D. C., Priestman, M., Canonaco, F., Coe, H., Prévôt, A. S. H., and Allan, J. D.: Organic aerosol source apportionment in London 2013 with ME-2: exploring the solution space with annual and seasonal analysis, Atmos. Chem. Phys., 16, 15545–15559, https://doi.org/10.5194/acp-16-15545-2016, 2016.

Riemer, N. and West, M.: Quantifying aerosol mixing state with entropy and diversity measures, Atmos. Chem. Phys., 13, 11423–11439, https://doi.org/10.5194/acp-13-11423-2013, 2013.

Salvador, P., Artinano, B., Querol, X., and Alastuey, A.: A combined analysis of backward trajectories and aerosol chemistry to characterize long-range transport episodes of particulate matter. The Madrid air basin, a case study, Sci. Total Environ., 390, 495–506, 2008.

Schichtel, B., Gebhart, K., Barna, M., and Malm, W.: Association of air mass transport patterns and particulate sulfur concentrations at Big Bend National Park, Texas, Atmos. Environ., 40, 992–1006, 2006.

Sun, C., Lee, B. P., Huang, D., Jie Li, Y., Schurman, M. I., Louie, P. K. K., Luk, C., and Chan, C. K.: Continuous measurements at the urban roadside in an Asian megacity by Aerosol Chemical Speciation Monitor (ACSM): particulate matter characteristics during fall and winter seasons in Hong Kong, Atmos. Chem. Phys., 16, 1713–1728, https://doi.org/10.5194/acp-16-1713-2016, 2016.

Sun, P., Nie, W., Chi, X., Huang, X., Ren, C., Xue, L., Shan, Y., Wen L., Li, H., Chen, T., Qi, Y., Gao, J., Zhang, Q., and Ding, A.: Aircraft study of secondary aerosols in long-range transported air masses from the North China Plain by a mid-latitude cyclone, J. Geophys. Res.-Atmos., 127, e2021JD036178, https://doi.org/10.1029/2021JD036178, 2022.

Sun, Y. L., Wang, Z. F., Fu, P. Q., Yang, T., Jiang, Q., Dong, H. B., Li, J., and Jia, J. J.: Aerosol composition, sources and processes during wintertime in Beijing, China, Atmos. Chem. Phys., 13, 4577–4592, https://doi.org/10.5194/acp-13-4577-2013, 2013.

Tang, G., Zhang, J., Zhu, X., Song, T., Münkel, C., Hu, B., Schäfer, K., Liu, Z., Zhang, J., Wang, L., Xin, J., Suppan, P., and Wang, Y.: Mixing layer height and its implications for air pollution over Beijing, China, Atmos. Chem. Phys., 16, 2459–2475, https://doi.org/10.5194/acp-16-2459-2016, 2016.

Tang, L., Eugensson, M., Sjöberg, K., and Wichmann, J.: Estimation of the long-range transport contribution from secondary inorganic components to urban background PM_{10} concentrations in south-western Sweden during 1986–2010, Atmos. Environ., 89, 93–101, 2014.

Tie, X. and Cao, J.: Aerosol pollution in China: Present and future impact on environment, Particuology, 7, 426–431, 2009.

Tie, X., Huang, R.-J., Dai, W., Cao, J., Long, X., Su, X., Zhao, S., Wang, Q., and Li, G.: Effect of heavy haze and aerosol pollution on rice and wheat productions in China, Sci. Rep., 6, 29612, https://doi.org/10.1038/srep29612, 2016.

Uno, I., Eguchi, K., Yumimoto, K., Takemura, T., Shimizu, A., Uematsu, M., Liu, Z., Wang, Z., Hara, Y., and Sugimoto, N.: Asian dust transported one full circuit around the globe, Nat. Geosci., 2, 557–560, 2009.

Wang, H., Wang, Q., Gao, Y., Zhou, M., Jing, S., Qiao, L., Yuan, B., Huang, D., Huang, C., Lou, S., Yan, R., Gouw, J., Zhang, X., Chen, J., Chen, C., Tao, S., An, J., and Li, Y.: Estimation of Secondary Organic Aerosol Formation During a Photochemical Smog Episode in Shanghai, China, J. Geophys. Res.-Atmos., 125, e2019JD032033, https://doi.org/10.1029/2019jd032033, 2020.

Xu, J., Tao, J., Zhang, R., Cheng, T., Leng, C., Chen, J., Huang, G., Li, X., and Zhu, Z.: Measurements of surface aerosol optical properties in winter of Shanghai, Atmos. Res., 109–110, 25–35, 2012.

Xu, J., Zhang, Q., Chen, M., Ge, X., Ren, J., and Qin, D.: Chemical composition, sources, and processes of urban aerosols during summertime in northwest China: insights from high-resolution aerosol mass spectrometry, Atmos. Chem. Phys., 14, 12593–12611, https://doi.org/10.5194/acp-14-12593-2014, 2014.

Xu, W., Xie, C., Karnezi, E., Zhang, Q., Wang, J., Pandis, S. N., Ge, X., Zhang, J., An, J., Wang, Q., Zhao, J., Du, W., Qiu, Y., Zhou, W., He, Y., Li, Y., Li, J., Fu, P., Wang, Z., Worsnop, D. R., and Sun, Y.: Summertime aerosol volatility measurements in Beijing, China, Atmos. Chem. Phys., 19, 10205–10216, https://doi.org/10.5194/acp-19-10205-2019, 2019.

Xue, J., Yu, X., Yuan, Z., Griffith, S. M., Lau, A. K. H., Seinfeld, J. H., and Yu, J. Z.: Efficient control of atmospheric sulfate production based on three formation regimes, Nat. Geosci., 12, 977–982, https://doi.org/10.1038/s41561-019-0485-5, 2019.

Yang, Y. R., Liu, X. G., Qu, Y., Wang, J. L., An, J. L., Zhang, Y., and Zhang, F.: Formation mechanism of continuous extreme haze episodes in the megacity Beijing, China, in January 2013, Atmos. Res., 155, 192–203, 2015.

Zhong, H.: Measurement report: On the contribution of long-distance transport to the secondary aerosol formation and aging, Zenodo [data set], https://doi.org/10.5281/zenodo.6446514, 2022.

Zhong, H., Huang, R., Duan, J., Lin, C., Gu, Y., Wang, Y., Li, Y., Zheng, Y., Chen, Q., Chen, Y., Dai, W., Ni, H., Chang, Y., Worsnop, D., Xu, W., Ovadnevaite, J., Ceburnis, D., and O'Dowd, C.: Seasonal variations in the sources of organic aerosol in Xi'an, Northwest China: the importance of biomass burning and secondary formation, Sci. Total. Environ., 737, 139666, https://doi.org/10.1016/j.scitotenv.2020.139666, 2020.